Environmental Science and Pollution Research (2018) 25:28961–28972
https://doi.org/10.1007/s11356-018-2929-7

RESEARCH ARTICLE

The impact of wetland on neutral mine drainage from mining wastes at Luanshya in the Zambian Copperbelt in the framework of climate change

Ondra Sracek[1] · Bohdan Kříbek[2] · Martin Mihaljevič[3] · Vojtěch Ettler[3] · Aleš Vaněk[4] · Vít Penížek[4] · Jan Filip[5] · František Veselovský[2] · Imasiku Nyambe[6]

Received: 15 April 2018 / Accepted: 6 August 2018 / Published online: 14 August 2018
© Springer-Verlag GmbH Germany, part of Springer Nature 2018

Abstract

The impact of a natural wetland ("dambo" in Zambia) on neutral mine drainage at Luanshya in the Zambian Copperbelt has been investigated during an intermediate discharge period (July) using a multi-method characterization of solid phase samples, sequential extraction analysis, X-ray diffraction, Mössbauer spectroscopy, and scanning electron microscopy combined with water analyses, isotopic analyses, and geochemical modeling. In the wetland, the principal identified solid phases in sediments were carbonates, gypsum, and ferric oxyhydroxides. A significant portion of the ochres was present as insoluble hematite. Mine drainage pH values decrease, and log P_{CO_2} values increase after inflow of water into the wetland; dissolved and suspended concentrations of Fe, Mn, Cu, and Co also decrease. Based on speciation calculations, there is no precipitation of secondary Cu and Co minerals in the period of sampling, but it can occur later in dry period when the flow rate is reduced. Concentrations of sulfate decrease, and values of $\delta^{34}S(SO_4)$ in the wetland increase in parallel, suggesting sulfate reduction is occurring. In more advanced dry period, the discharge in mine drainage stream is probably much lower and water can reach supersaturation with respect to minerals such as gypsum, which has been found in sediments. Wetlands have a positive impact on mine drainage water quality due to the removal of metals by adsorption, co-precipitation, and filtration of colloids. However, there can also be a rebound of contamination by seepage inflow downstream from the wetland. Ongoing climate change with extreme hydrologic events may enhance differences between dry and rainy seasons with resulting faster mobilization of contaminants.

Keywords Neutral mine drainage · Ochres · Wetland · Adsorption · Climate change · Zambia

Responsible editor: Philippe Garrigues

✉ Ondra Sracek
srondra@seznam.cz

Bohdan Kříbek
bohdan.kribek@geology.cz

Martin Mihaljevič
mihal@natur.cuni.cz

Vojtěch Ettler
ettler@natur.cuni.cz

Aleš Vaněk
vaneka@af.czu.cz

Vít Penížek
penizek@af.czu.cz

Jan Filip
jan.filip@upol.cz

František Veselovský
frantisek.veselovsky@geology.cz

Imasiku Nyambe
inyambe@gmail.com

[1] Department of Geology, Faculty of Science, Palacký University, 17. listopadu 12, 771 46 Olomouc, Czech Republic

[2] Czech Geological Survey, Klárov 3, 118 21 Prague, Czech Republic

[3] Institute of Geochemistry, Mineralogy and Mineral Resources, Faculty of Science, Charles University, Albertov 6, 128 43 Prague, Czech Republic

[4] Department of Soil Science and Soil Protection, Faculty of Agrobiology, Food and Natural Resources, Czech University of Life Sciences Prague, Kamýcká 129, 165 00 Prague 6, Czech Republic

[5] Regional Centre of Advanced Technologies and Materials, Palacky University, Šlechtitelů 27, 78371 Olomouc, Czech Republic

[6] Department of Geology, School of Mines, University of Zambia, P.O. Box 32 379, Lusaka, Zambia

Introduction

Oxidation of sulfidic minerals in mining wastes can result in mine drainage with low pH and high concentrations of sulfate, iron, and other metals and metalloids (Blowes et al. 2003). When significant fractions of carbonates such as calcite and dolomite are embedded in gangue rocks, resulting mine drainage can be neutral and concentrations of dissolved species are much lower (Sracek et al. 2012; Kruse et al. 2013).

In neutral mine drainage, there can be significant amounts of ferric because ferric hydroxide precipitates at a pH level > 3.0 in the reaction

$$Fe^{2+} + 0.25O_2 + 2.5H_2O = Fe(OH)_3 + 2H^+ \quad (1)$$

which form ferric ochres at the stream bottom and mobile particles which adsorb and/or co-precipitate other contaminants (Kimball et al. 1995; Schemel et al. 2007; Consani et al. 2017). The mineralogy of ochres depends on pH and mine drainage chemistry, forming a sequence with increasing pH starting with jarosite, schwertmannite, goethite, and ferrihydrite (Bingham et al. 1996). Precipitated ferric colloids transported by water may increase the mobility and bioavailability of metals and metalloids (Wang and Gou 2000; Meunier et al. 2010; Sarmiento et al. 2012). Aquatic plants in wetlands located along the streams draining the mining wastes contribute to the attenuation of metals by adsorption, stabilization, and filtering of colloidal particles (Kumpiene et al. 2008; Nyquist and Greger 2009) and may also provide organic matter necessary for dissolved sulfate reduction (Appelo and Postma 2005). They also provide surfaces for precipitation of ferric phases (Eq. (1)) and stabilize precipitated ochres, which can be transformed later to more crystalline and less soluble phases such as goethite and hematite (Sracek et al. 2011).

In countries with seasonal distribution of precipitation such as those in the Sub-Saharan region of Africa, an accumulation of efflorescent salts during the dry period is followed by their dissolution and a fast contaminant input at the beginning of the rainy period (Sracek et al. 2010; Anawar 2015). Ongoing climate change results in extreme hydrological events such as high intensity of precipitation (Green et al. 2011), and there can be a larger contaminant pulse caused by intense rain.

We studied neutral mine drainage from old (more than 70 years) Cu-Co mine tailings at Luanshya in the Zambian Copperbelt (Fig. 1a). The mine drainage stream flows through a wetland with aquatic plants, and well-developed ferric ochres are found in the stream sediments (Fig. 1b). The region is characterized by high temperature and extremely seasonal changes in precipitation. The objectives were to (1) evaluate the impact of wetland on mine drainage geochemistry and to (2) determine the role of ochres and colloids in the attenuation of mine drainage contaminants, especially Cu.

Site description

The Luanshya site is located in Northern Zambia in the so-called Copperbelt (Fig. 1a). There are rocks of the Katanga system formed in the Neoproterozoic age, forming a part of the Lufilian Arc (Mendelsohn 1961). Principal rocks are argillaceous and carbonate shale, limestone, and dolomite of the Upper Roan, Mwashia, Katonkwe, and Kundelungu formations (Rainaud et al. 2005). Mining is located mostly in the Lower Roan Formation with pyrite (FeS_2), chalcopyrite ($CuFeS_2$), bornite (Cu_5FeS_4), linnaeite (Co_3S_4), and carrollite ($Cu(Co,Ni)_2S_4$) embedded in carbonate-rich shale, argillite, and sandstone as principal ore minerals. The average ore grade is 3 wt% for Cu and 0.18 wt% for Co (Kamona and Nyambe 2002).

The Luanshya deposit is at the eastern end of the Katangan rocks synclinorium. The ore formation composed of dolomitic argillite is 15–50 m thick. The mineral sequence begins with chalcocite and bornite at the bottom with increasing contents of chalcopyrite and pyrite upward (Dixon 1979). Exploitation of the deposit has been developed through mining shafts and large stopes. The ore was concentrated by flotation and smelted. The treatment resulted in the accumulation of large mine tailings. The study site is a part of the Chonga Dam constructed in the 1930s and 1940s, where the upper part of the tailings has been oxidized. A creek flows from the dam, which is located in the depression cut into the mine tailings (Fig. 1a). Ferric ochres are developed along the creek (Fig. 1b), and some seepage also comes from the side slopes of the depression (Fig. 1c).

In the Copperbelt, there are three climate seasons: a rainy season from November to April, a cold-dry season from May to June, and a hot-dry season from August to October. Almost all of the total precipitation of more than 1300 mm falls during the rainy season when discharge in surface streams reaches extreme values. Wetland depressions with aquatic plants and surrounded by miombo woodland and located on surface streams are called “dambo” in Zambia (“vlei” in South Africa and Namibia) and may play a significant role in the attenuation of mine drainage (Sracek et al. 2011).

Material and methods

Sampling of stream sediments and water

Sampling profile SP1 was located on the slope of mine tailings in the proximity of seepage (Fig. 1a). Samples of stream

Fig. 1 **a** Site map with location of sampling points. **b** Outflow from the wetland with precipitated ochres. **c** Seepage hole at the creek bottom close to sampling point S4

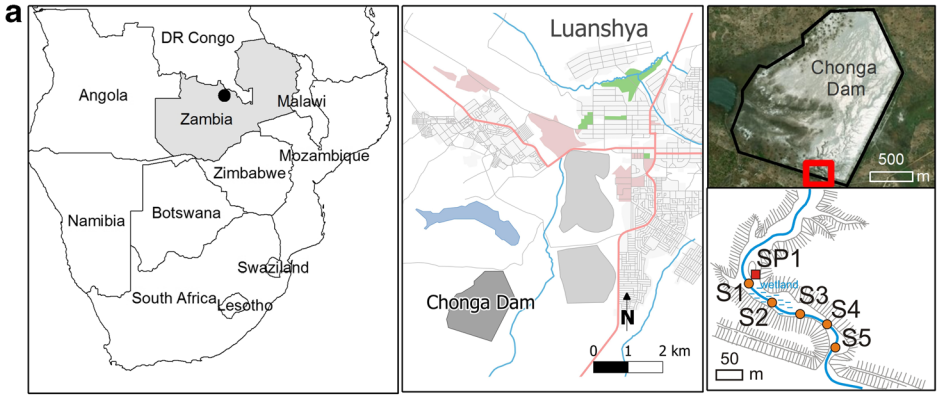
a
DR Congo
Angola
Malawi
Zambia
Mozambique
Zimbabwe
Namibia
Botswana
Swaziland
South Africa
Lesotho
Luanshya
Chonga Dam
N
0 1 2 km
Chonga Dam
500 m
SP1
S1
wetland
S2
S3
S4
S5
50 m


b

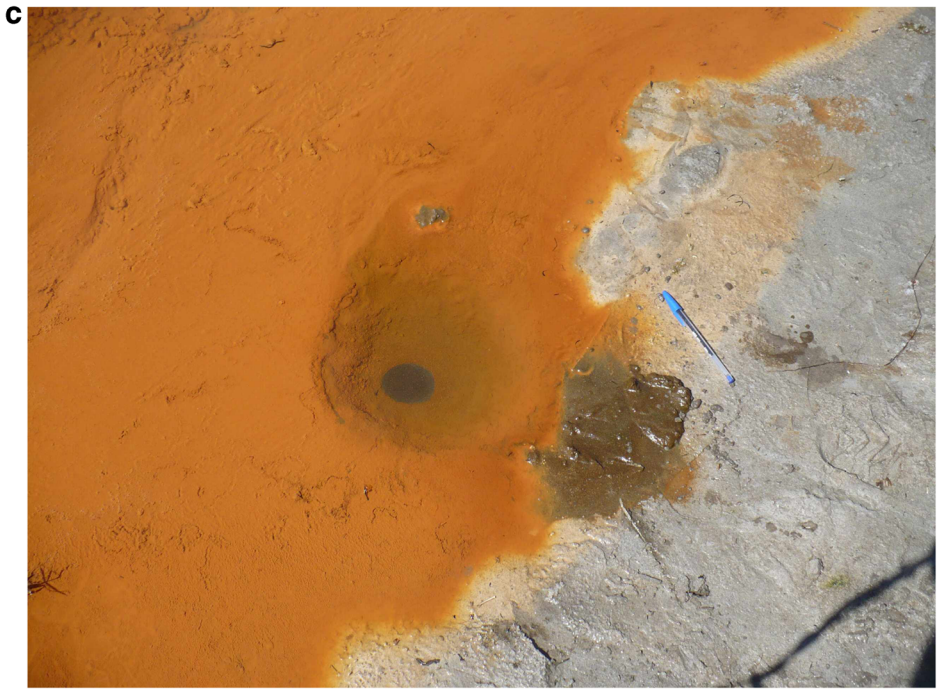
c

sediments at points from S1 to S5 were taken with a plastic spoon from the upper ca. 1 cm. The samples were packed in polyethylene (PE) bags. Mine drainage water was sampled from stream originating from seepage face at the base of mine tailings. Flow rate estimated using weir was about 2 l/s. The following field parameters: temperature, pH, Eh, and electrical conductivity (EC) were measured on-site. Water was filtered through 0.45-μm filters, then acidified for cation and trace element analyses by ultrapure HNO_3 and collected in PET bottles. Second, water sample was only acidified, but not filtered, to determine a difference in concentrations between dissolved and colloidal trace elements. Samples for anion analyses were filtered, but not acidified. Cations were analyzed by FAAS and anions by HPLC (Dionex ICS 2000). Simultaneously, samples of stream sediments including precipitated ochres were taken using a spatula and also packed in PE bags. Sampling was performed in early July 2017, i.e., in the middle of dry period, and was focused on species present in principal ore-forming minerals present at the site.

Bulk composition of solid samples

The pseudo-total digests of samples were obtained by a standardized *aqua regia* extraction protocol in accordance with the ISO 11466 procedure (International Organization for Standardization 1995). All reagents were declared *pro analysi*, and all solutions were prepared using double-distilled water. Heavy metals and metalloids were determined using flame atomic absorption spectroscopy (FAAS; Perkin-Elmer 4000 spectrometer). Certified reference material (CRM 7001, sandy soil) was used to control the accuracy of the aqua regia pseudo-total digestion, yielding reproducibility values below 10%.

X-ray powder diffraction of heavy fractions of sediments

The X-ray powder diffraction (XRD) analyses were performed with a PANalytical X'Pert instrument (CoKα radiation, 40 kV/40 mA) equipped with an X'Celerator detector and programmable incident and diffracted beam anti-scatter slits. Samples were placed on zero-background Si slides, gently pressed in order to obtain sample thicknesses of about 0.5 mm, and scanned at a near-constant irradiation volume in the 2θ range of 3–65° in steps of 0.017° for 5.83 s per step. Results were interpreted by the program ZDS (Ondruš 1993).

^{57}Fe Mössbauer spectroscopy

Transmission ^{57}Fe Mössbauer spectra of samples S1 (before wetland) and S2 (in the wetland), powdered in an agate mortar, were collected in constant acceleration mode with a ^{57}Co (Rh) source (1.85 GBq) at room temperature. The spectrum was fitted by Lorentz functions using the computer program CONFIT2000, v. 4.6.24.0 (Žák and Jirásková 2006). Isomer shift values were calibrated against an α-Fe foil at room temperature. The effects of non-ideal absorber thickness and variable recoil-free fractions for iron atoms in non-equivalent structural sites of different phases were expected to be within the experimental error of the technique (hyperfine parameters ± 0.02 mm/s, relative spectral area ± 2%).

Electron microscopy

The detailed morphological study of solid phases was done on a field emission scanning electron microscope (FE-SEM; Hitachi SU6600) with ultra-high point-to-point resolution (1–2 nm) and equipped with electron-dispersive X-ray (EDX) spectroscopy.

Sequential extraction

Sequential extractions for selected bulk sediment samples were performed using the BCR procedure (Rauret et al. 1999). The following extraction scheme was used: a 0.11 M acetic acid (CH_3COOH) step targeting exchangeable and acid soluble fractions, a 0.5 M hydroxylamine-hydrochloride ($NH_2OH{\cdot}HCl$) step targeting the reducible fraction (mostly poorly crystalline iron/manganese oxides), an oxidizable step (8.8 M H_2O_2/1 M CH_3COONH_4 extractable) targeting organic matter and sulfides, and an aqua regia step targeting the residual fraction. The detailed experimental scheme is given by Rauret et al. (1999).

Stable isotopes in water analyses

Samples for stable isotopes of water were stored in airtight sealed glass bottles. Isotope values $\delta^{18}O$ and $\delta^{2}H$ in water were determined at the Czech Geological Survey using a Los Gatos Research laser absorption spectrometer. Sulfate sulfur from waters was precipitated with $BaCl_2$ (in hot solution acidified with HCl to pH 3.5) as $BaSO_4$ which was decomposed with a mixture of V_2O_5, SiO_2, and Cu at 1000 °C in a vacuum to SO_2. The reproducibility of $\delta^{34}S$ preparation and measurement is ± 0.25‰. Calibration of the laboratory standard was carried out by the IAEA international standards (NZ1 and NZ2) and the recommended comparative materials (NBS122 and NBS127).

Geochemical modeling

Speciation calculations were performed by the program PHREEQC (Parkhurst and Appelo 1999) using the database minteq.dat. The solubility diagram for Cu was constructed in the Geochemist's Workbench Professional 7.0 program.

Results

Solid phase composition

Total solid phase contents of selected elements are shown in Table 1. The Fe contents increase from 22,279 mg/kg before the wetland to a maximum of 35,294 mg/kg in the middle of the wetland and then decrease downstream. Contents of Ca are slightly lower in the wetland compared to the maximum of 39,376 mg/kg at the wetland entry. Contents of both Cu and Co reach maximum respective values of 1839 mg/kg and 169 mg/kg in the wetland. Total contents in mine tailings which were analyzed on sample SP1 collected a few meters from the stream (Fig. 1a) are also shown in Table 1. Contents of Fe and Ca are more than 20,000 mg/kg. Content of Cu is 1329 ppm and is 1 order of magnitude higher than Co content, reaching 159 mg/kg.

Sequential extraction results are reported in Fig. 2. Maximum Fe content was generally found in the aqua regia fraction (F4) followed by reducible fraction (F2) and oxidizable fraction (F3). The acid extractable fraction (F1) is almost non-existent. The sample S2 from the wetland is an exception because the maximum of Fe is in reducible fraction (F2). There is almost equal distribution of Cu among fractions (Fig. 2b) with a maximum acid extractable fraction (F1) in sample S1 before the wetland. Distribution of Co (Fig. 2c) is similar to that of Cu with a maximum in the reducible fraction (F2) in sample S2 in the wetland.

Results of X-ray diffraction for representative samples are shown in Fig. 3, and relative abundances of minerals are shown in Table 2. Calcite occurs in large amounts in all samples. Quartz plus silicates such as albite and muscovite are also abundant. Traces of gypsum were found in samples S1–S3. No ferric minerals were detected, but an upward shift of baseline (Fig. 2a, b) suggests the presence of amorphous ferric phases such as ferrihydrite. No discrete mineral phases of Cu such as malachite and Co such as $Co(OH)_3$ were detected.

In order to shed light into the character of Fe-bearing phases, we also performed Mössbauer spectroscopy on the isotope ^{57}Fe of two samples (S1 and S2; Fig. 4). In sample S1 (i.e., sediment upstream from the wetland), 55% of iron atoms are in the oxidation state 3+, partially in the form of hematite (23% of iron atoms from Fe_{tot}) and amorphous superparamagnetic iron oxides/oxyhydroxides (32% of iron atoms from Fe_{tot}; cf., Filip et al. 2007). The rest of the iron atoms (45% from Fe_{tot}) are in the oxidation state 2+ with hyperfine parameters of the respective spectral component (doublet) typical for Fe^{2+} in silicates—which could therefore indicate Fe^{2+} in detrital biotite as identified by XRD. In sample S2 (i.e., sediment from wetland), iron atoms are predominantly in oxidation 3+ in the form of amorphous superparamagnetic iron oxides/oxyhydroxides (71% of iron atoms from Fe_{tot}) and partially in the oxidation state 2+ (29%; similarly as in the case of sample S1) and we ascribe this component to detrital silicates like biotite. The significant increase of the Fe^{3+} component in sample S2 (compared to

Table 1 Total contents of selected elements in ppm

Element/ sample	Fe	Ca	Cu	Co
S1	22,279	39,376	1597	124
S2	35,294	27,841	1839	169
S3	29,074	30,586	1829	138
S4	26,649	25,546	1303	124
S5	8700	7825	488	69
SP1	20,304	28,166	1329	159

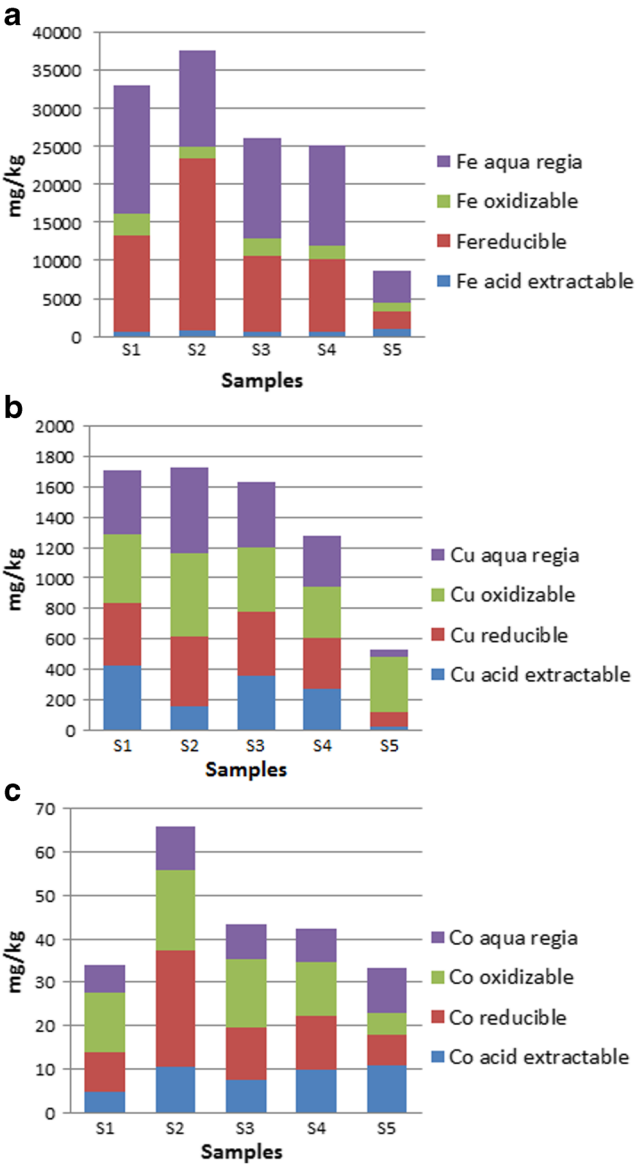

Fig. 2 Sequential extraction results for selected elements. **a** Fe. **b** Cu. **c** Co

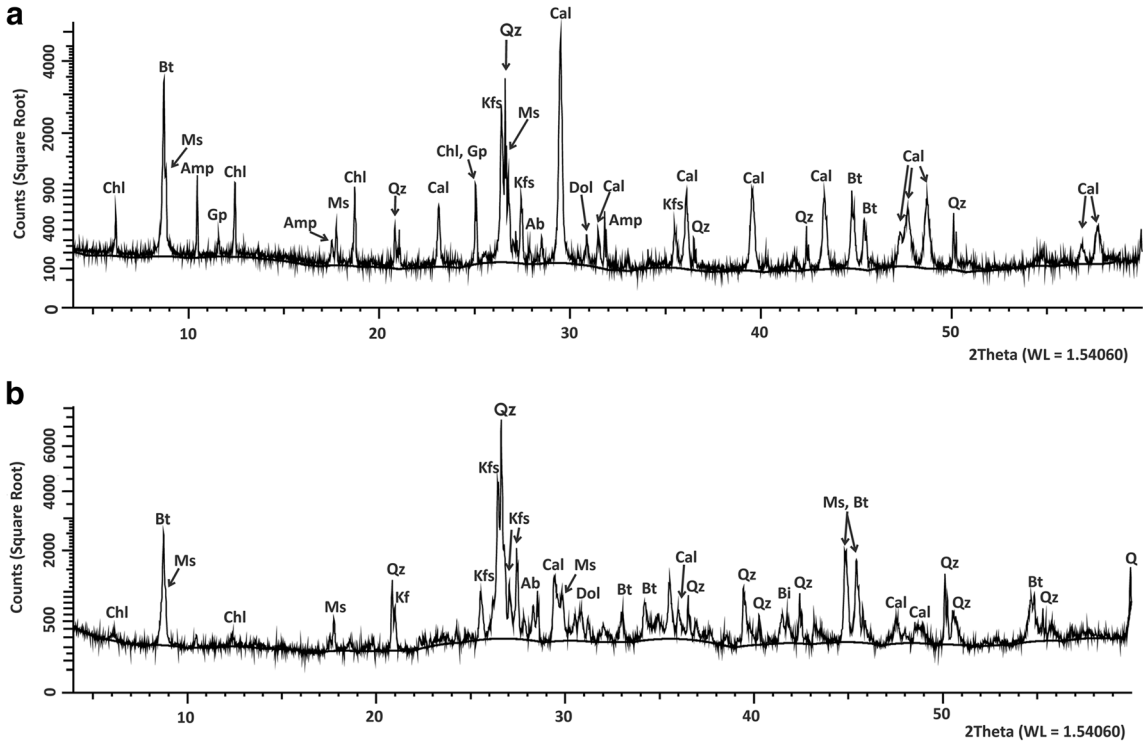

Fig. 3 Representative results of X-ray diffraction. **a** S1. **b** S4. Legend: Qz quartz, Cal calcite, Chl chlorite, Dol dolomite, Amp amphibole, Ab albite, Bt biotite, Ms muscovite, Gp gypsum, Kfs K-feldspar

sample S1) could indicate enhanced precipitation of ferric oxyhydroxides in the wetland. The particle size and morphology of the iron-bearing phases are shown in Fig. 5—the combination of FE-SEM and EDX analysis confirmed the nanocrystalline character of the ferric oxyhydroxides (most particles/aggregates are in the range of 100 to 200 nm) overgrowing larger fragments of detrital minerals.

Water chemistry and isotopes

Water chemistry parameters are given in Fig. 6. Values of pH drop from 7.8 at the wetland entrance to 7.2 in the middle of the wetland and then increase downstream to the last sampling point where pH reaches 8.2 (Fig. 6a). Values of Eh corrected with respect to the hydrogen electrode (not shown) were in the range 560–660 mV. Sulfate concentrations decrease from 543 mg/l at the wetland entrance to 472 mg/l in the wetland and then increase again to 494 mg/l at the last sampling point. Concentrations of HCO_3 increase in the wetland to 302 mg/l and then decrease downstream (Fig. 6b).

There is a sharp decrease of both dissolved and colloidal Mn and Fe in the wetland (Fig. 6c). Respective dissolved concentrations of Mn and Fe decrease from 7.37 mg/l and 8.49 mg/l at the wetland entry to 1.15 mg/l and 0.106 mg/l in the middle of wetland. Much more Fe is transported in

Table 2 Semi-quantitative abundances of minerals based on X-ray diffraction

Mineral/sample	Quartz	Calcite	Chlorite	Amphibole	Albite	Muscovite	Gypsum	Dolomite	Biotite	K-feldspar
S1	3	4	1	2	3	2	1	2	3	1
S2	4	3	1	1	2	3	1	nd	5	2
S3	4	3	1	1	4	3	1	nd	5	3
S4	5	3	1	2	3	4	nd	nd	5	3
S5	4	4	2	5	4	3	nd	nd	4	4

5 = maximum; 1 = minimum

nd not detected

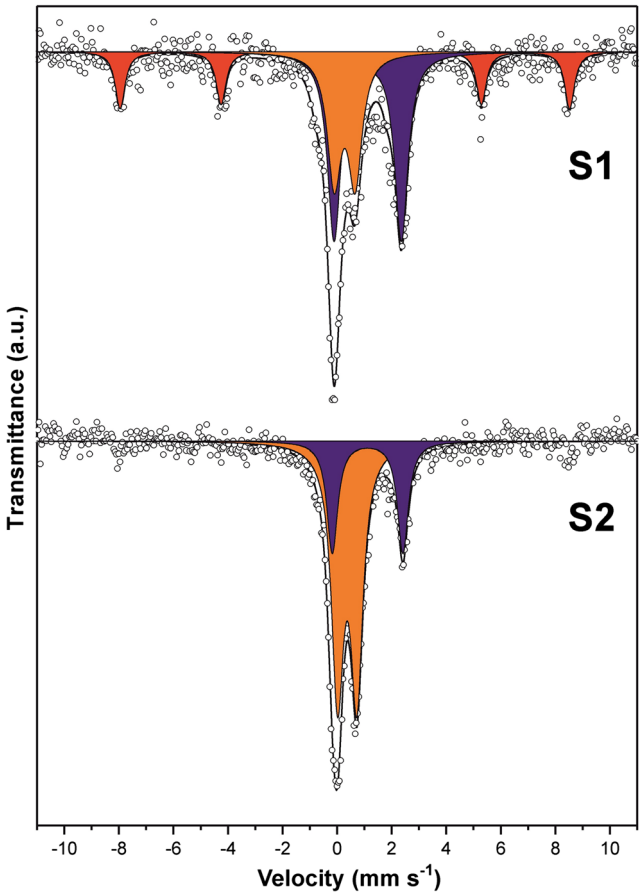

Fig. 4 ^{57}Fe Mössbauer spectra collected from samples S1 (before wetland) and S2 (wetland). The various oxidation states/phases are marked by different colors of respective spectral components: orange, Fe^{3+} in superparamagnetic phase; purple, Fe^{2+}; red, Fe^{3+} in hematite (α-Fe_2O_3)

colloidal form compared to Mn. There is a moderate rebound of both Mn and Fe concentrations downgradient from the wetland.

The same trends are observed for Co and Cu (Fig. 6d). Concentrations of Co are always higher than those of Cu, but much less Co is transported as a colloidal fraction. Again, there is a moderate rebound of both contaminant concentrations after wetland.

Values of stable isotopes of δ^2H vs. $\delta^{18}O$ are plotted with the local meteoric water line (LMWL) for Ndola in the vicinity of Luanshya in Fig. 7a. All samples are affected by evaporation, but no particular trend along the stream has been identified. Evaporation plays an important role in concentrating mine drainage waters (Nordstrom 2009) and may result in the precipitation of efflorescent salts in tropical and subtropical regions (Sracek et al. 2010).

Values of $\delta^{34}S(SO_4)$ vs. SO_4 are plotted in Fig. 7b. Upgradient of the wetland, the value of $\delta^{34}S(SO_4)$ corresponds to values typical for oxidation of sulfides (Thurston et al. 2010). Downstream samples S2 and S3 collected in the wetland show enriched $\delta^{34}S(SO_4)$ values up to +30‰ and lower sulfate concentrations compared to initial sample S1, suggesting sulfate reduction is occurring (Clark 2015). There are more depleted $\delta^{34}S(SO_4)$ values of about +15‰ and higher concentrations of sulfate downstream after the wetland, suggesting the input of isotopically depleted SO_4 from lateral seepage at the bottom of the creek.

Speciation modeling

Selected results of speciation modeling are reported in Table 3. All samples are supersaturated with respect to calcite and dolomite and also with respect to ferric phases like ferrihydrite and goethite. On the other hand, water is undersaturated with respect to gypsum and all Cu-bearing minerals. Some samples are close to saturation with $Co(OH)_3$, and considering a possible analytical error, precipitation of this phase is possible. There is an increase of log P_{CO_2} in sample S2 in the wetland to − 1.77, but values return to − 2.85 at the last sampling point (S5) downstream of the wetland.

Principal dissolved species of Cu are, in decreasing order, as follows: $CuCO_3 > Cu(CO_3)_2^{2-} > CuOH^+ > Cu^{2+}$. Principal dissolved species of Co are as follows: $Co^{2+} > CoSO_4 > CoHCO_3^+ > CoCO_3 > CoOH^+$.

Discussion

Mine drainage at the study site has a neutral character due to a high content of carbonates in the solid phase. The impact of wetlands on mine drainage has been studied by several researchers, especially in relation to the construction of artificial wetlands for removal of dissolved metals, metalloids, and sulfate (Johnson and Hallberg 2005; Nyquist and Greger 2009). The principal processes in wetlands include (a) adsorption of metals and metalloids on organic matter, plants, and precipitated ferric oxyhydroxides; (b) settlement of colloidal and suspended material due to lower flow rates in the wetlands; (c) reduction of sulfate and precipitation of secondary sulfites co-precipitating dissolved metals and metalloids; and (d) decomposition of organic matter and precipitation of carbonate phases due to increased alkalinity. Macrophytes and their roots provide surfaces for precipitation of ferric oxyhydroxides and stabilize accumulated ochres (Kalin 2001; Johnson and Hallberg 2005; Sracek et al. 2011; Kříbek et al. 2011). Seasonal changes occur in the composition of ochres when more crystalline phases, e.g., goethite, are formed from less crystalline phases, e.g., ferrihydrite or schwertmannite during warmer period (Kumpulainen et al. 2007). Fast transformation of low-crystallinity ferric phases into more crystalline phases was also found in mine tailings in Namibia (Sracek et al. 2014).

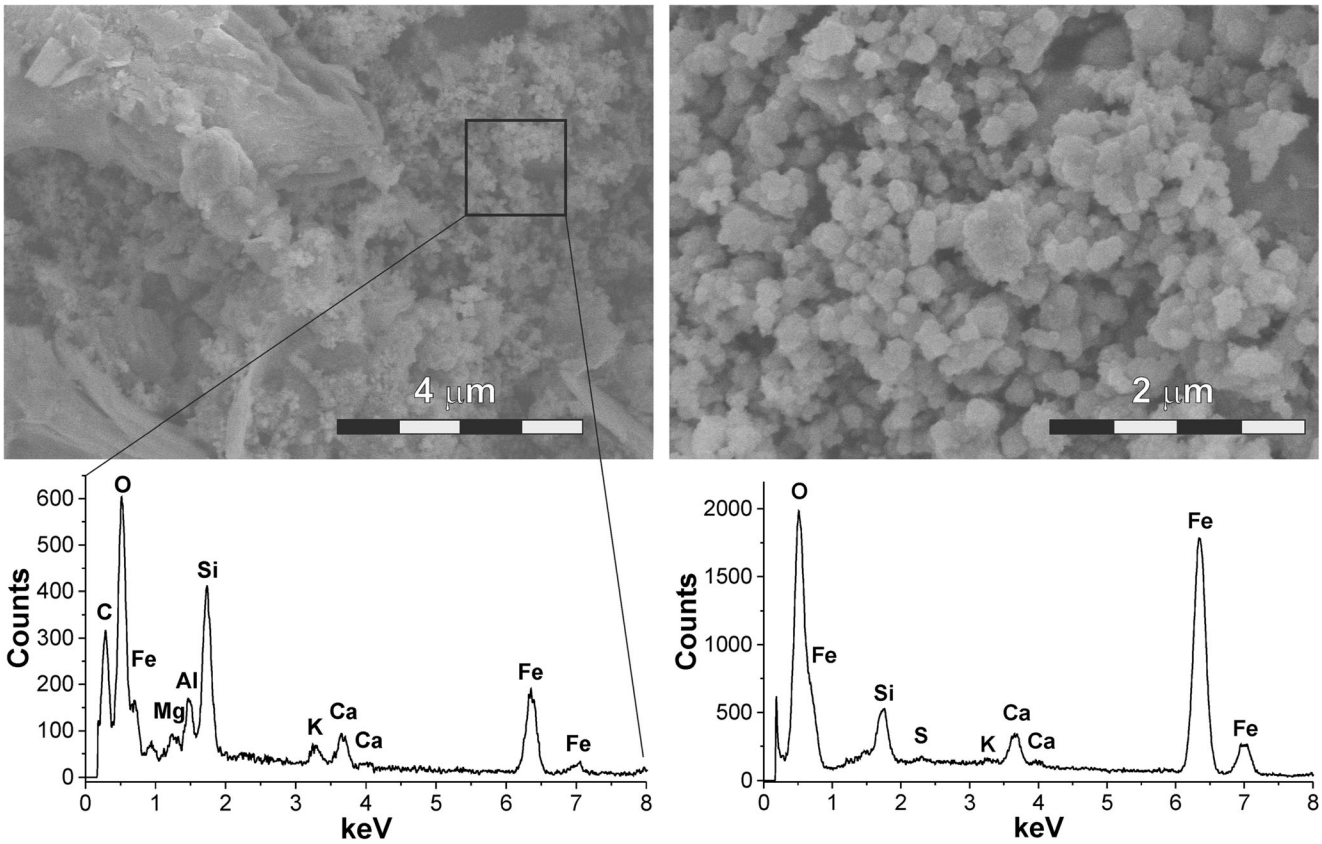

Fig. 5 FE-SEM images of samples S1 (left) and S2 (right) with corresponding EDX spectra (the EDX spectrum for sample S2 was collected from the whole visible area above)

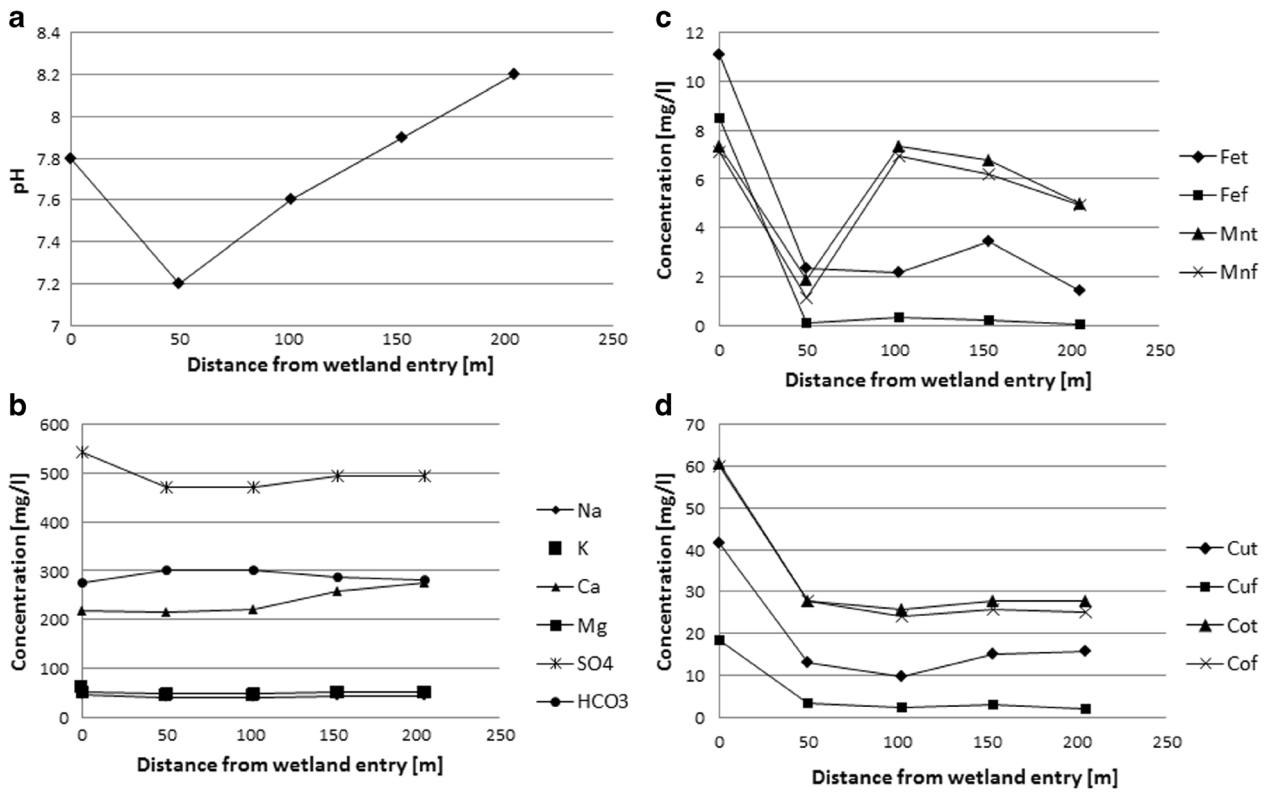

Fig. 6 Water chemistry profiles for selected parameters. **a** pH. **b** Principal ions. **c** Fe and Mn (t total, f filtered). **d** Cu and Co (t total, f filtered)

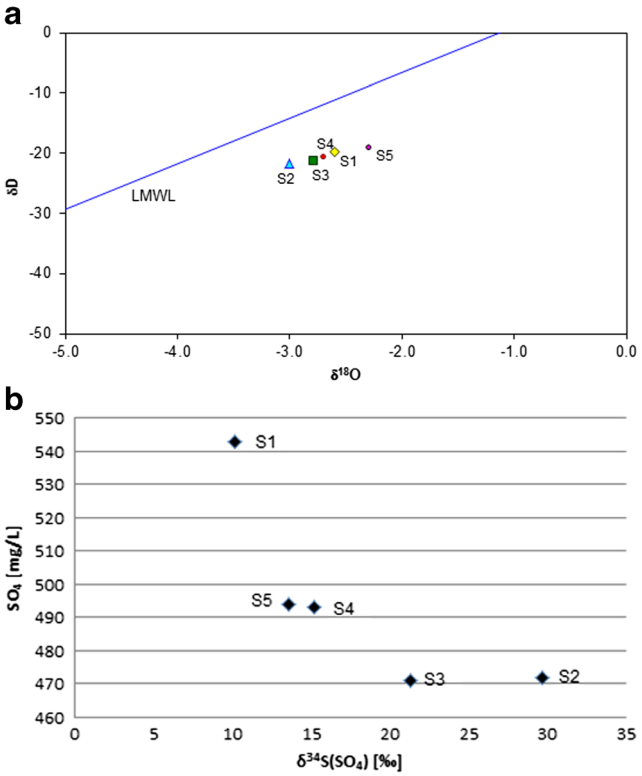

Fig. 7 Isotopic results. **a** Plot of δ^2H vs. $\delta^{18}O$, the meteoric water line: $\delta^2H = 6.1\delta^{18}O + 6.9$ is for Ndola (GNIP 2017). **b** Plot of $\delta^{34}S(SO_4)$ vs. SO_4; sample S1 is upstream, samples S2 and S3 are from the wetland, and samples S4 and S5 are downstream of the wetland

The abovementioned processes seem to be operating at the study site. Dissolved and colloidal Fe concentrations decrease in the wetland, where large amounts of nanocrystalline ferric oxyhydroxides precipitate (Figs. 4 and 5). The Mössbauer spectroscopy indicates a significant portion of ferric phases (up to 23%) as insoluble hematite. Both colloidal and dissolved Cu concentrations decrease by 60–90% in sample S2 in the wetland compared to the inflow sample S1. However, removal of Co is less efficient and reaches about 50% of initial concentrations. Based on enriched $\delta^{34}S(SO_4)$ values (up to 33‰), sulfate reduction takes place in the wetland (Fig. 7b). A significant oxidizable fraction of both Cu and Co (Fig. 2b, c) suggests a presence of sulfidic minerals, but some of them can be primary tailing material. Generally, based on Eh values, conditions in free-flowing water in the wetland are oxidizing, but sulfate reduction can occur at discrete sites with a large amount of organic matter and in the root zone of aquatic plants. Also, pH in the wetland decreases (Fig. 6a) and log P_{CO_2} increases (Table 3) presumably as a consequence of organic matter decomposition.

Downstream of the wetland, an increase in sulfate concentration and a decrease in $\delta^{34}S(SO_4)$ values are close to the values upstream of the wetland. Two factors probably contribute to the observed sulfate behavior. First, stream bottom seepage probably occurs from the sides of the drainage stream (Fig. 1c) which contributes sulfate and colloidal and dissolved Fe, Mn, Cu, and Co to the mine drainage creek. Enriched values of δ^2H and $\delta^{18}O$ (Fig. 7a) indicate evaporation (Clark and Fritz, 1997), but no particular trend along sampling sites has been identified.

Gypsum was found in stream sediments (Table 2), but water was undersaturated with respect to the mineral (Table 3). No minerals of Cu and Co were found, but it is not surprising due to low sensitivity of X-ray diffraction. Relatively significant acid-extractable fractions of Cu and Co (Fig. 2b, c) suggest the presence of carbonate minerals such as malachite which was undetected by low sensitivity of X-ray diffraction. The solubility diagram for Cu is plotted in Fig. 8.

In the diagram, the region of field Cu data acquired from the intermediate flow regime in July is well below the stability boundaries of Cu-bearing minerals. This is consistent with results of speciation calculations (Table 3) and suggests adsorption and co-precipitation with secondary ferric phases as principal Cu and Co attenuation processes (Jönsson et al. 2006). Both processes cannot be separated, but adsorption-only-based models generally underpredict removal of contaminants (Miller et al. 2013). Strong seasonal variations of mine drainage chemistry caused by hydrologic variations were found also in the Iberian Pyrite Belt in Spain and at Rodalquilar in SE Spain, where climatic conditions are similar to the Copperbelt (España et al. 2005; Gonzáles et al. 2012; Nieto et al. 2013).

Flow rates in the Copperbelt streams decrease dramatically in late September, and supersaturation with respect to gypsum

Table 3 Selected results of speciation modeling

SI value/sample	Calcite	Dolomite	$Co(OH)_3$	$Cu(OH)_2$	Ferrihydrite	Goethite	Gypsum	Malachite	Log P_{CO_2}
S1	*0.86*	*1.45*	−0.36	−1.46	*5.11*	*7.81*	−0.69	−0.86	−2.43
S2	*0.32*	*0.36*	−1.87	−2.90	*2.76*	*5.46*	−0.73	−3.06	−1.77
S3	*0.92*	*1.55*	−0.75	−2.34	*3.66*	*6.37*	−0.72	−2.74	−2.37
S4	*1.05*	*1.78*	−0.54	−2.16	*3.57*	*6.27*	−0.65	−2.34	−2.32
S5	*1.35*	*2.35*	−0.04	−2.11	*2.26*	*4.96*	−0.64	−2.50	−2.85

Values presented in italics indicate supersaturation

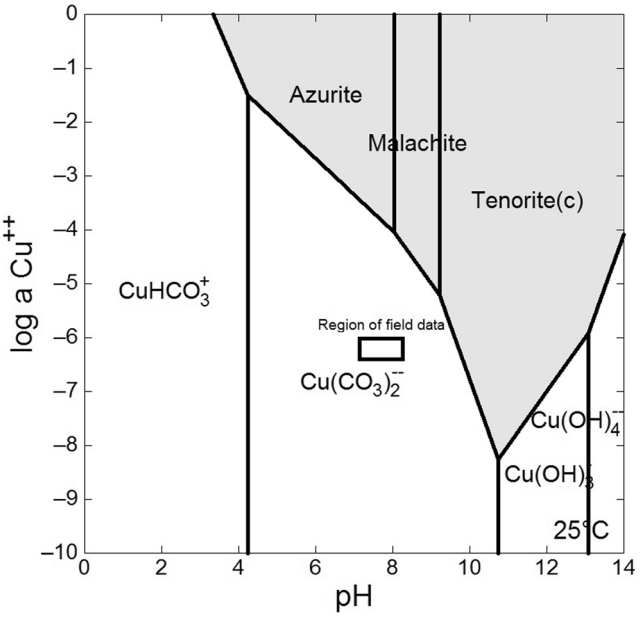

Fig. 8 Speciation of Cu vs. pH diagram constructed for average concentrations of Cu^{2+}, SO_4^{2-}, and HCO_3^- in the stream; gray color indicates the stability field of mineral phases

and also Cu carbonates is probably reached. In contrast, discharge increases in the rainy period (November–March) by several orders of magnitude as observed in the Kafue River (Petterson and Ingri 2001; von der Heyden and New 2003; Sracek et al. 2012).

In this period, some precipitated minerals can be washed out, but can be replenished during the next dry period. Ongoing climate change and rising temperatures with resulting higher evaporation rate (Green et al. 2011) may produce larger amounts of precipitated minerals in dry season followed by their faster mobilization during intense storms at the beginning of rainy season (Nordstrom 2009).

Conclusions

The impact of a natural wetland (dambo) on neutral mine drainage at Luanshya, the Zambian Copperbelt, has been studied during the intermediate flow period, aiming to identify principal attenuation processes. In the wetland, the principal identified solid phase sediments were carbonates, gypsum, and amorphous ferric oxyhydroxides. Mössbauer spectroscopy indicated greater amounts of ferric phases in the wetland compared to the wetland inflow zone and a significant portion of ochres (up to 23%) as insoluble hematite. Values of pH decrease, log P_{CO_2} values increase after inflow of water into the wetland, and dissolved and suspended concentrations of Fe, Mn, Cu, and Co also decrease. Based on speciation calculations, precipitation of any secondary Cu and Co minerals does not occur during the sampling period and the principal attenuation processes probably are adsorption and co-precipitation. However, precipitation may occur later in the dry period when the flow rate is reduced. In the wetland, concentrations of sulfate decrease and values of $\delta^{34}S(SO_4)$ increase in parallel, suggesting sulfate reduction is occurring reducing. Increasing sulfate concentrations downstream of the wetland are probably caused by the inflow of water from the surrounding tailings into the stream. Our study was performed in the middle of dry period (early July), but precipitation of phases like gypsum can occur in the low discharge/advanced dry period in September and their redissolution occurs at the high flow rate during the rainy period starting in November. Ongoing climate change can result in greater amounts of precipitated minerals in the dry period followed by faster mobilization of contaminants at the beginning of the rainy period. These findings might be applicable to other countries with similar climate conditions in Africa, South America, and Southeastern Asia.

Acknowledgments The authors also acknowledge the assistance provided by the Research Infrastructure NanoEnviCz, supported by the Ministry of Education, Youth and Sports of the Czech Republic under project no. LM2015073. Part of the equipment used for this study was purchased under the Operational Programme Prague – Competitiveness (Project CZ.2.16/3.1.00/21516). This study was supported by the Czech Science Foundation project (16-13142S) and projects no. LM2015073 and institutional funding from the Center for Geosphere Dynamics (UNCE/SCI/006). The authors thank the journal editor and anonymous reviewers for their comments, which helped to improve the manuscript.

References

Anawar HM (2015) Sustainable rehabilitation of mining waste and acid mine drainage using geochemistry, mine type, mineralogy, texture, ore extraction and climate knowledge. J Environ Manag 158:111–121. https://doi.org/10.1016/j.jenvman.2015.04.045

Appelo CAJ, Postma D (2005) Geochemistry groundwater and pollution, 2nd edn. Balkema, A.A, p 649

Bigham JM, Schwertmann U, Pfab G (1996) Influence of pH on mineral speciation in a bioreactor simulating acid mine drainage. Appl Geochem 11:845–849. https://doi.org/10.1016/S0883-2927(96)00052-2

Blowes, D.W., Ptacek, C.J., Jambor, J.L., Weisener, C.G., 2003. The geochemistry of acid mine drainage, In: Lollar B.S. (Ed.), Environmental geochemistry, treatise on geochemistry, Vol. 9, Elsevier, 149–204

Clark, I., 2015. Groundwater, geochemistry and isotopes, CRC, p. 438

Clark, I., Fritz, P., 1997. Environmental isotopes in hydrogeology, Lewis, p. 328

Consani S, Carbone C, Dinelli E, Balić-Žunić T, Cutroneo L, Capello M, Salviulo G, Luchetti G (2017) Metal transport and remobilisation in a basin affected by acid mine drainage: the role of ochreous amorphous precipitates. Environ Sci Polut Res 24(18):15735–15747. https://doi.org/10.1007/s11356-017-9209-9

Dixon, C.J., 1979. The Luanshya Copper Deposit—Zambia, atlas of economic mineral deposits, Chapman and Hall Ltd, p. 42

España JS, Pamo EL, Santofimia E, Aduvire O, Reyes J, Barettino D (2005) Acid mine drainage in the Iberian Pyrite Belt (Odiel river watershed, Huelva, SW Spain): geochemistry, mineralogy and environmental implications. Appl Geochem 20:1320–1356. https://doi.org/10.1016/j.apgeochem.2005.01.011

Filip J, Zboril R, Schneeweiss O, Zeman J, Cernik M, Kvapil P, Otyepka M (2007) Environmental applications of pure natural ferrihydrite. Env Sci Technol 41:4367–4374. https://doi.org/10.1021/es062312t

GNIP, 2017. Global networks of isotopes in precipitation and rivers: https://nucleus.iaea.org/Pages/GNIPR.aspx

Gonzáles V, García I, del Moral F, de Haro S, Sánchez JA, Simón M (2012) Spreading of pollutants from alkaline mine drainage. Rodalquilar mining district (SE Spain). J Environ Manag 106:69–74. https://doi.org/10.1016/j.jenvman.2012.04.011

Green TR, Taniguchi M, Kooi H, Gurdak JJ, Allen DM, Hiscock KM, Treidel H, Aureli A (2011) Beneath surface of global change: impacts of climate change on groundwater. J Hydrol 405:532–560. https://doi.org/10.1016/j.jhydrol.2011.05.002

Johnson DB, Hallberg KB (2005) Acid mine drainage remediation options: a review. Sci Tot Environ 338:3–14. https://doi.org/10.1016/j.scitotenv.2004.09.002

Jönsson J, Jönsson J, Lövgren L (2006) Precipitation of secondary Fe(III) minerals from acid mine drainage. Appl Geochem 21:437–445. https://doi.org/10.1016/j.apgeochem.2005.12.008

Kalin M (2001) Biogeochemical and ecological considerations in designing wetland treatment systems in post-mining landscapes. Waste Manag 21:191–196. https://doi.org/10.1016/S0956-053X(00)00063-5

Kamona, A.F., Nyambe, I.A., 2002. Geological characteristics and genesis of stratiform sediment-hosted Cu-(Co) deposits, Zambian Copperbelt, In: Proceedings of the 11th IAGOD Quadrennial Symposium and Geocongress, Extended Abstracts (R.E. Miller, editor), Geological Survey of Namibia, Windhoek, Namibia

Kimball BA, Callender E, Axtmann EV (1995) Effects of colloids on metal transport in a river receiving acid mine drainage, upper Arkansas River, Colorado, USA. Appl Geochem 10:285–306. https://doi.org/10.1016/0883-2927(95)00011-8

Kříbek B, Mihaljevič M, Sracek O, Knésl I, Ettler V, Nyambe I (2011) The extent of arsenic and of metal uptake by aboveground tissues of *Pteris vittata* and *Cyperus* involucratus growing in copper- and cobalt-rich tailings of the Zambian Copperbelt. Archives Environ Contam Toxicol 61:228–242. https://doi.org/10.1007/s00244-010-9604-4

Kruse NA, DeRose L, Korenowsky R, Bowman JR, Lopez D, Johnson K, Rankin E (2013) The role of remediation, natural alkalinity sources and physical stream parameters in stream recovery. J Environ Manag 128:1000–1011. https://doi.org/10.1016/j.jenvman.2013.06.040

Kumpiene J, Lagerkvist A, Maurice C (2008) Stabilization of As, Cr, Cu, Pb and Zn in soil using amendments—a review. Waste Manag 28:215–225. https://doi.org/10.1016/j.wasman.2006.12.012

Kumpulainen S, Carlson L, Räisänen M-L (2007) Seasonal variations of ochreous precipitates in mine effluents in Finland. Appl Geochem 22:760–777. https://doi.org/10.1016/j.apgeochem.2006.12.016

Mendelsohn F (1961) The geology of the Northern Rhodesian Copperbelt. Macdonald and Co., London, p 523

Meunier L, Walker SR, Wragg J, Parson MB, Koch I, Jamieson HE, Reimer KJ (2010) Effects of soil composition and mineralogy on the bioaccessibility of arsenic from mine tailings and soil in gold mine district of Nova Scotia. Environ Sci Technol 44:2667–2674. https://doi.org/10.1021/es9035682

Miller A, Wildeman T, Figueroa L (2013) Zinc and nickel removal in limestone based treatment of acid mine drainage: the relative role of adsorption and co-precipitation. Appl Geochem 37:57–63. https://doi.org/10.1016/j.apgeochem.2013.07.001

Nieto JM, Sarmiento AM, Canovas CR, Olias M, Ayora C (2013) Acid mine drainage in the Iberian Pyrite Belt: 1. Hydrochemical characteristics and pollutant load of the Tinto and Odiel rivers. Environ Sci Polut Res 20(11):7509–7519. https://doi.org/10.1007/s11356-013-1634-9

Nordstrom DK (2009) Acid rock drainage and climate change. J Geochem Explor 100:97–104. https://doi.org/10.1016/j.gexplo.2008.08.002

Nyquist J, Greger M (2009) A field study of constructed wetlands for preventing and treating acid mine drainage. Ecol Engin 35:630–642. https://doi.org/10.1016/j.ecoleng.2008.10.018

Ondruš P, 1993 ZDS—a computer program for analysis of X-ray powder diffraction patterns. Materials Science Forum, pp. 133–136. 297–300, EPDIC-2. Enschede

Parkhurst DL, Appelo CAJ, 1999. User's guide to PHREEQC; a computer program for speciation, reaction-path, 1-D transport and inverse geochemical calculations, U.S. Geological Survey Water Resources-Investigations Report 99–4259

Petterson UT, Ingri J (2001) The geochemistry of Cu and Co in the Kafue River as it drains the Copperbelt mining area, Zambia. Chem Geol 177:399–414. https://doi.org/10.1016/S0009-2541(00)00422-8

Rainaud C, Masters S, Armstrong RA, Robb LJ (2005) Geochronology and nature of the Palaeoproterozoic basement in the Central African Copperbelt (Zambia and the Democratic Republic of Kongo), with regional implications. J Afr Earth Sci 42:1–32. https://doi.org/10.1016/j.jafrearsci.2005.08.006

Rauret G, Lopez-Sanchez JF, Sahuquillo A, Rubio R, Davidson C, Ure A, Quevauviller P (1999) Improvement of the BCR three step sequential extraction procedure prior to the certification of new sediment and soil reference materials. J Environ Monit 1:57–61. https://doi.org/10.1039/A807854H

Sarmiento AM, Caraballo MA, Sanchez-Rodas D, Nieto JM, Parviainen A (2012) Dissolved and particulate metals and arsenic species mobility along a stream affected by acid mine drainage in the Iberian Pyrite Belt (SW Spain). Appl Geochem 27:1944–1952. https://doi.org/10.1016/j.apgeochem.2012.07.012

Schemel LE, Kimball BA, Runkel RL, Cox MH (2007) Formation of mixed Al–Fe colloidal sorbent and dissolved-colloidal partitioning of Cu and Zn in the Cement Creek—Animas River Confluence, Silverton, Colorado. Appl Geochem 22:1467–1484. https://doi.org/10.1016/j.apgeochem.2007.02.010

Sracek O, Veselovský F, Kříbek B, Malec J, Jehlička J (2010) Geochemistry, mineralogy and environmental impact of precipitated efflorescent salts at the Kabwe Cu-Co chemical leaching plant in Zambia. Appl Geochem 25:1815–1824. https://doi.org/10.1016/j.apgeochem.2010.09.008

Sracek O, Filip J, Mihaljevič M, Kříbek B, Majer V, Veselovský F (2011) Attenuation of dissolved metals in neutral mine drainage in the Zambian Copperbelt. Environ Monitor Assess 172:287–299. https://doi.org/10.1007/s10661-010-1334-6

Sracek O, Kříbek B, Mihaljevič M, Majer V, Veselovský F, Vencelides Z, Nyambe I (2012) Mining-related contamination of surface water and sediments of the Kafue River drainage system in the Copperbelt district, Zambia: an example of a high neutralization capacity system. J Geoch Explor 112:174–188. https://doi.org/10.1016/j.gexplo.2011.08.007

Sracek O, Mihaljevič M, Kříbek B, Majer V, Filip J, Vaněk A, Penížek V, Ettler V, Mapani B (2014) Geochemistry of mine tailings and behavior of arsenic at Kombat, northeastern Namibia. Environ. Monitor. Assess. 186:4891–4903. https://doi.org/10.1007/s10661-014-3746-1

Thurston RS, Mandernack KW, Shanks WC III (2010) Laboratory chalcopyrite oxidation by *Acidithiobacillus ferrooxidans*: oxygen and

sulfur isotope fractionation. Chem Geol 269:252–261. https://doi.org/10.1016/j.chemgeo.2009.10.001

Von der Heyden CJ, New MG (2003) The role of a dambo in the hydrology of a catchment and the river network downstream. Hydrol Earth Syst Sciences 7:339–367. https://doi.org/10.5194/hess-7-339-2003

Wang WX, Guo L (2000) Influences of natural colloids on metal bioavailability to marine bivalves. Environ Sci Technol. 34:4571–4457. https://doi.org/10.1021/es000933v

Zak T, Jiraskova Y (2006) CONFIT: Mössbauer spectra fitting program. Surf Interface Anal 38:710–714. https://doi.org/10.1002/sia.2285